This is a peer-reviewed, accepted author manuscript of the following research article: Köksal, ÇS, Aktas, B, Gürkan, AY, Sasaki, N & Atlar, M 2024, 'Experimental assessment of hull, propeller, and the gate rudder system interaction in calm water and oblique waves', Ocean Engineering, vol. 312, no. Pt. 2, 119144. https://doi.org/10.1016/j.oceaneng.2024.119144

Experimental Assessment of Hull, Propeller, and the Gate Rudder System Interaction in Calm Water and Oblique Waves

Çağatay Sabri Köksal[a, *], Batuhan Aktas[a], Ahmet Yusuf Gürkan[a], Noriyuki Sasaki[a], Mehmet Atlar[a]

[a] *Naval Architecture, Ocean and Marine Engineering, University of Strathclyde, Glasgow, United Kingdom*

Abstract

This study focuses on the experimental assessment of the EU H2020 Innovation Action project GATERS' target ship, a 7241 DWT multi-purpose dry cargo ship (M/V ERGE), scaled to 1/27.1, in calm water and oblique wave (at a yaw angle of the ship model) conditions. M/V ERGE was initially built with a Conventional Rudder System (CRS) in 2010 but was later retrofitted with a newly introduced energy-saving device, the Gate Rudder System (GRS), in 2023 as part of the GATERS project. In this project, the interaction of the GRS with the hull and propeller was investigated using model tests of the vessel in the Kelvin Hydrodynamics Laboratory's (KHL) towing tank at the University of Strathclyde (UoS) and compared to the CRS. The main objectives of these tests were threefold. While they aimed to make experimental contributions toward the establishment of the best procedure for estimating the powering prediction of a ship with the GRS, they also aimed to investigate the hull, propeller and rudder interaction for the CRS and GRS configurations. In addition, a set of comparative pilot tests were conducted in waves to explore the effect of the oblique waves on the vessel's performance with the CRS and GRS. The resistance and self-propulsion tests were performed for both the CRS and GRS configurations, and performance predictions based on the model tests were compared with sea trials. Furthermore, tests at a yaw angle of the ship model were conducted to evaluate the effect of waves on the vessel's performance with the CRS and GRS, simulating the in-service conditions of commercial ships. These tests were conducted in regular waves with the hull at a yaw angle to simulate oblique wave conditions, with a wave height of 1.25 meters in full scale (corresponding to moderate breeze, Beaufort 4) for a range of wavelengths. Numerical analyses were performed to obtain the full-scale propeller open water characteristics. The paper demonstrates the superior interaction of the GRS with the hull and propeller in both conditions compared to the CRS configuration, even improving its contribution to the vessel's performance in oblique waves.

Keywords

Hull, Propeller and Rudder Interaction; Gate Rudder System; Ship Model Tests; Oblique Waves

Nomenclature

C_A	Correlation allowance	k_s	Roughness of hull surface
C_{AA}	Air resistance coefficient	n	Propeller rate of revolution
C_F	Frictional resistance coefficient	P_E	Effective power
C_T	Total resistance coefficient	R_e	Reynolds number
F_D	Skin friction correction	w	Taylor wake fraction
J	Propeller advacnce coefficient	t	Thrust deduction factor
K_T	Propeller thrust coefficient	ΔC_F	Roughness allowance
K_Q	Propeller torque coefficient	η_0	Propeller open water efficieny
k	Form factor	λ	Wavelength
ω	Wave (absolute) frequency	ω_e	Encounter wave frequency

1. Introduction

In order to contribute to the global greenhouse gas emissions (GHG) reduction for the sake of climate change, the International Maritime Organization (IMO) adopted the first set of international mandatory measures to improve ships' energy efficiency in 2011. Since then, IMO has taken additional action including further regulatory measures, the adoption of the Initial IMO GHG strategy in 2018, and, in 2023, the revised Strategy on Reduction of GHG Emissions from Ships. To support their implementation, IMO executes a comprehensive capacity-building and technical assistance programme, including a range of global projects. Therefore, implementing energy-saving devices, one of the potential solutions for ensuring energy efficiency and reducing carbon footprint is very important for ship owners. Various technology solutions have emerged in this respect, including retrofitting ships with energy-saving devices like the Gate Rudder System (GRS). The EU H2020 Innovation Action project GATERS (GATERS, 2021) focuses on implementing the GRS on a 90 meters 7241 DWT multi-purpose dry cargo ship (M/V ERGE) to demonstrate its emission reduction potential Sasaki et al. (2016).

Energy-saving devices improve flow characteristics (Mewis et al., 2011) and can be classified based on their location or working principles. Ducts are one type of energy-saving device and include variations such as the wake-equalising duct (Schneekluth, 1989), the Mewis duct (Mewis, 2009), the Becker-Mewis duct (Guiard et al., 2013), the Mitsui Integrated Duct Propeller (MDIP) and the Hitachi Zosen Nozzle (HZN). These ducts reduce the cavitation risk on propellers and improve a ship's propulsion performance and manoeuvrability (Kitazawa et al., 1982). Another type of energy-saving device is the pre-swirl stator (PSS), which is located upstream of the propeller and used to recover rotational energy losses. The purpose of the PSS devices is to increase propeller efficiency and improve the wake (Simonsen et al., 2012). The GRS consists of two asymmetric rudders on each side of a propeller and can be considered an open-type ducted propeller rather than a ducted propeller. The GRS generates lift and provides additional thrust due to the duct effect of the rudder blades, improving propulsive efficiency and reducing propeller loading. As a result, the GRS offers improved propulsion characteristics, leading to reduced propeller-hull interaction. The flow field around the GRS is relatively uniform, with minimal disturbance from the propeller slipstream, and the average flow speed at the GRS blades is close to the ship speed (Sasaki et al., 2020). This configuration reduces flow separation and streamlines the flow upstream and downstream of the propeller, thereby improving propeller efficiency.

The GRS features a twin rudder arrangement, unlike the conventional rudder system (CRS), replacing the single rudder configuration behind the propeller with individually controlled twin rudders positioned on either side of the propeller. The GRS blades generally generate lift; however, at large angles of attack and very high speeds, they may produce drag instead of lift, similar to ducted propellers. The interaction between the propeller and GRS is typically favourable, though less pronounced compared to CRS, shifting the stall angle at larger angles (GATERS, 2022). The GRS' steering gear can be operated at larger rudder angles, depending on its operational mode, such as open sea, port, bollard pull, and astern operations, compared to the CRS. In order to ensure that the GRS does not exceed the rudder angle limits based on operational mode and ship speed, the autopilot and steering gear are configured to operate within a set permissible range, thereby preventing any exceedance of these limits. This permissible rudder angle range is determined based on both hydrodynamic and structural analyses. This novel arrangement offers tremendous

advantages over the CRS. A comprehensive investigation of the early version of the GRS, known as the twin rudder system, was first conducted by Sasaki et al. (2016). Based on the initial assessment, it was seen that the state-of-the-art GRS has superiorities in propulsion (Turkmen et al., 2015), manoeuvrability (Carchen et al., 2021) and seakeeping (Sasaki et al., 2019) characteristics, and underwater radiated noise (URN) mitigation (Sasaki, 2022). The GRS concept was first applied to the 450 TEU and 2400 GT container ship, SHIGENOBU, where its performance was compared with those of her sistership, SAKURA, equipped with the CRS through sea trials and voyage monitoring. These trials indicated that SHIGENOBU achieved 14% lower fuel consumption than SAKURA at the service speed, and up to 30% energy savings in rough seas, demonstrating the GRS' potential to improve energy efficiency (Sasaki et al., 2020).

In recent years, both experimental and numerical studies have been conducted to investigate the effects of the GRS on various aspects, including ship powering performance, seakeeping, maneuverability, propeller cavitation, and underwater radiated noise (URN). Many of these studies have specifically focused on enhancing powering performance and achieving energy savings in ships. Turkmen et al. (2015) carried out a series of tests in the Emerson Cavitation Tunnel (ECT) and measured and compared the forces on the GRS and CRS behind the ship. All of these measurements were conducted at the model scale, and the open water data for the propeller with GRS around it were obtained from these open water tests. The measurements show that the GRS rudder blades generates additional thrust with the increased rotational rate of the propeller, while the conventional rudder generates additional frictional force. Turkmen et al. (2015) found 4-8% higher thrust deduction (t) in propulsion tests with GRS compared to CRS. Also, in the comparative analysis of the open water data for a propeller with a gate rudder and a conventional rudder, a 15-25% higher wake fraction (w) value was obtained with the GRS. Turkmen et al. (2015) also investigated the effect of full-scale GRS on the aft flow field by CFD analysis. It was observed that when the gate rudder was placed closer to the propeller plane (at 1.25×R compared to 1.50×R), there was a 10% increase in thrust force. Sasaki et al. (2016) conducted an experimental and computational study on the application of the GRS for a large bulk carrier. The forces on the gate rudder were measured, and it was shown that the GRS presented a thrust of 6% of the hull resistance. The study indicated that the gate rudder provides an energy saving of 7-8% and would amortise the investment cost within 0.37-0.9 years. In the recently completed EU-H2020 project GATERS (2021), Köksal et al. (2022) examined the results of the resistance, propulsion, and seakeeping experiments conducted with the GATERS target ship (M/V ERGE) model at the Kelvin Hydrodynamics Laboratory (KHL) of the University of Strathclyde. In the calm water resistance experiment, the model with GRS reduced the hull resistance by 4% compared to the model with CRS. In the propulsion test, the GRS improved the delivered power by over 10% compared to the hull with CRS. Seakeeping tests were conducted in regular waves to simulate oblique wave conditions. A comparison of the powering performance of the vessel with the CRS and GRS revealed that torque was 20% less for the GRS than that in the model the CRS. Çelik et al. (2022) extrapolated the model test results for 2400 TEU Containership obtained from the Ata Nutku Ship Model Testing Laboratory's towing tank of Istanbul Technical University to full scale using various methods. Comparing these extrapolated results with the sea trials data, the method where the GRS was considered as an appendage showed better agreement. The powering predictions indicated that the GRS configuration could reduce the power requirement by 2% at the service speed compared to the CRS configuration under full-loaded conditions. As part of the GATERS project investigations, Mizzi et al. (2022) demonstrated the assessment of CFD methods,

solvers, and approaches used to accurately predict the performance of the ships with GRS. Specifically, simulations at the model scale were conducted for the M/V ERGE ship using two different turbulence models, and the obtained results were validated with experimental data. Tacar et al. (2020) conducted an experimental and numerical study to investigate the effect on ship performance of a container ship equipped with GRS for full and trial load. Experimental and numerical studies were carried out with models of 2 m and 5 m, and the scale effect was examined. Tacar et al. (2020) demonstrated that as the speed of the vessel increased, the advantageous effect of the GRS became more pronounced compared to the CRS at the trial conditions. Furthermore, they highlighted that at a service speed of 15 knots, the ship equipped with the GRS required approximately 17% less brake power compared to the one fitted with a CRS. The authors found that concerning scale effects, the smaller model tends to overpredict, whereas the larger model tends to underpredict the power requirement when compared to sea trial measurements. Çelik et al. (2023) analysed the results of three different sea trials data for the M/V ERGE ship to examine the accuracy of extrapolating model test measurements to full scale. Additional frictional resistance due to ageing and fouling effects was included in the full-scale extrapolation, and the results were compared with those of the sea trial. The analysis revealed that during the January 2023 trials, M/V ERGE experienced a 21% increase in power with the CRS at a speed of 11.5 knots due to ageing and fouling conditions. On the other hand, the optimisation studies for improving the powering performance of the GRS were presented in Gürkan et al. (2023 a), Gürkan et al. (2023 b), and Gürkan et al. (2023 c) within the framework of the GATERS project. In addition to these studies on powering performance and energy efficiency, there has also been a focus on investigating the effects of the GRS on manoeuvrability. Sasaki et al. (2017), Fukuzawa et al. (2018), Carchen et al. (2021), and Gürkan et al. (2023 d) presented their studies involving various aspects of manoeuvrings of the ships with GRS. Turkmen et al. (2018), Özsayan et al. (2023), Santic et al. (2023), Köksal et al. (2023 a), Köksal et al (2023 b), Köksal et al (2023 c) and Köksal et al. (2024) also conducted experimental and numerical investigations involving the cavitation, URN and detailed flow analyses of ships with the GRS. Recently, Sasaki and Atlar (2024) claimed that the GRS could offer significant design advantages and, hence, the development of new hull forms, which could be more advantageous. Their study introduced four applications emphasising, namely, (i) how the GRS-equipped ships could eliminate the higher CAPEX cost of the GRS with savings in hull steel weight; (ii) being complementary for vessels to be fitted with WASP (wind-assisted ship propulsion) in providing effective counterbalancing heel/yawing moments; (iii) presenting reduced URN and; (iv) offering potentially the best solution for resolving the contradiction between EEDI 'Phase 3' and MPP requirements. Bulten (2024) conducted full-scale CFD studies of a bulk carrier equipped with the GRS and also examined scenarios expected to arise when this ship is equipped with a WASP. To cover a broader operating range, a dynamic system simulation model based on the CFD dataset was developed. This model provides ship operating conditions (such as ship speed and external forces) to encompass a broader range of operational scenarios.

This study provides an up-to-date literature review focused on GRS technology. The procedures for model tests and sea trials were explained. A comparison of model test results extrapolated to the full scale and sea trials for both the CRS and GRS configurations was made. The forces acting on the rudder blades at the same model speed in various propeller speeds and at the self-propulsion points were presented. The rudder on both the CRS and GRS configurations were measured in calm water and oblique waves and then compared for the first time to assess the hull, propeller and

rudder interaction. The forces on both GRS rudder blades, on the port and starboard sides, were presented separately to assess the performance of each rudder blade at a yaw angle of the ship model in oblique waves. Propeller open water simulations were conducted at full scale, and the results were compared with the model test results extrapolated to full-scale using standard methods and the design data used for the propeller retrofitted on the vessel, M/V ERGE. The discussions were expanded, leading to conclusions about the hull, propeller, and rudder interaction. The main objectives of this study are to make experimental contributions toward the best procedure for estimating the powering prediction of a ship with the GRS, to investigate the hull, propeller and rudder interaction for both the CRS and GRS configurations, and to conduct comparative tests in waves to explore the effect of oblique waves on vessel's performance in both configurations. In achieving these objectives, Section 2 of the paper presents the experimental facility, equipment, details on the experimental setup, the test matrix, and the sea trials. Section 3 provides the results and discussions of the tests conducted in calm water and oblique waves (at a yaw angle of the ship model). Finally, Section 4 offers concluding remarks based on these investigations.

2. Model Tests, Numerical Analyses and Sea Trials

2.1 Model test setup

A ship model (Fig. 1) with a scale of 1/21.7 of the target vessel M/V ERGE was built following the ITTC procedure (2017 a). This model was used in resistance and calm water/oblique wave self-propulsion tests in the Kelvin Hydrodynamics Laboratory (KHL) towing tank (Fig. 2 a) at the University of Strathclyde (UoS). The hydrostatic particulars of the vessel, M/V ERGE, for both the model scale and full scale, are provided in Table 1.

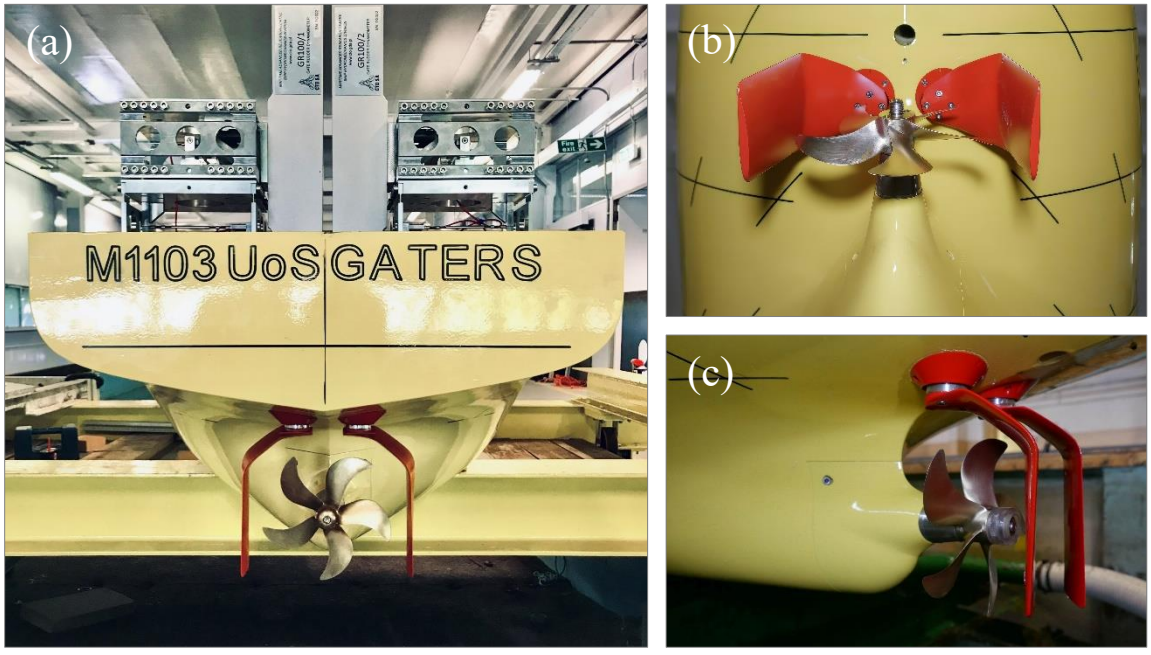

Fig. 1 (a) Stern, (b) bottom and (c) side view of the ship with the GRS.

Table 1. Main particulars of M/V ERGE (the numbers are rounded to three decimal places).

Characteristics	Symbol	Model	Ship
Length, overall	L_{OA} (m)	4.145	89.950
Length, between perp.	L_{PP} (m)	3.915	84.950
Beam	B_{WL} (m)	0.710	15.400
Draught (midship)	T (m)	0.152	3.3000
Displacement	Δ (ton)	0.363	3585.0
Block coeff.	C_B	0.806	0.8060
Prismatic coeff.	C_P	0.823	0.8230
Midship coeff.	C_M	0.994	0.9940
Waterplane area coeff.	C_{WP}	0.854	0.8540

The propeller model (Fig. 2 b), with geometric features detailed in Table 2, was used for both the CRS and GRS self-propulsion tests, as well as the propeller open water tests. This propeller model was scaled from the newly designed propeller for M/V ERGE, which was installed as part of the GRS retrofit on the vessel in 2023 within the GATERS project activities (GATERS, 2021). The propeller model was manufactured with a tolerance of ±0.027 mm at the same scale factor as the ship model, 1/21.7, following the ITTC procedure (2017 a), where the diameter of the propeller model is approximately 0.17 meters. Propeller open water characteristics were measured to be used both to obtain the self-propulsion coefficients and to extrapolate the model scale test results. The ship model incorporated an interchangeable stern part (Fig. 1 c) that enabled interchanging the CRS and GRS aft end configurations. The towing tank has the dimensions of 76×4.6×2.6 (L×B×H) meters, and the maximum carriage speed is up to 5 m/s. The carriage operates using a computer-controlled digital drive system. The wavemaker is a computer-controlled, four-flap type device that generates regular or irregular waves over 0.5 meters in height (subject to water depth). It features a high-quality, variable-water-depth sloping beach with a reflection coefficient typically less than 5% across the frequency range of interest.

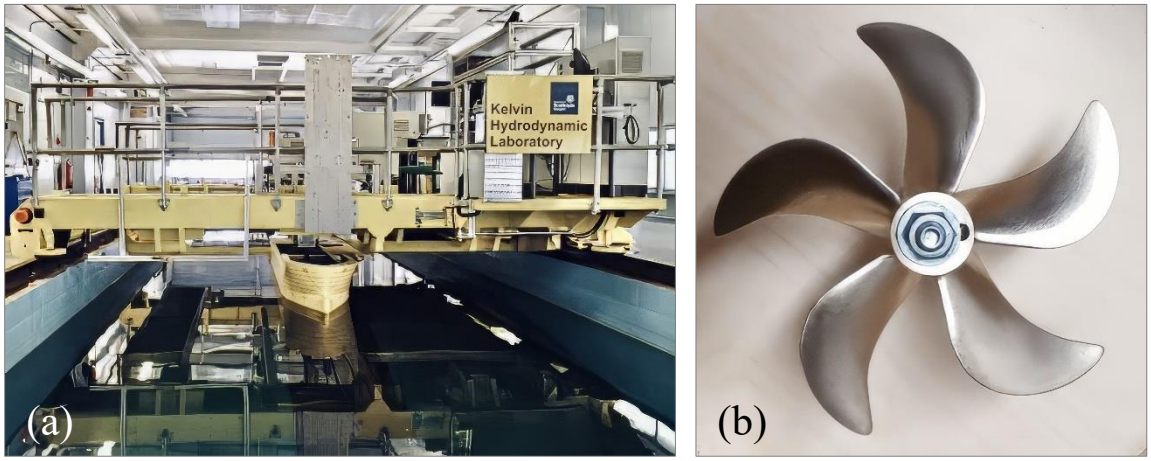

Fig. 2 (a) Ship model attached to the carriage, (b) propeller model.

Table 2. Main particulars of propeller model.

Characteristics	Model
Number of blades	5
Blade area ratio (BAR)	0.4551
Diameter (D)	0.1659
Pitch ratio ($P_{0.7}$/D)	0.83
Material	Brass
Direction of rotation	Left-handed

The ship model was free to trim and sinkage during the calm water and oblique wave tests. A custom-made measurement mechanism, including a load cell and its components, was designed and tailor-made to measure forces and moments acting on both rudder blades, the CRS and GRS, and to adjust the rudder blade angles (Fig. 3). The setup of the measurement device for the CRS and GRS configurations are shown in Fig. 3 (a) and Fig. 3 (b, c), respectively. This experimental setup is specifically built to assess the interaction of rudder blades with the propeller and the hull in detail under various conditions. A self-propulsion dynamometer and its remaining components were commissioned to measure the propeller thrust and torque and to adjust the propeller speed, up to 50 1/s with a 1.5 kW rated power, having 250 N thrust and 10 Nm torque measurement capacity with a capacity of 50% higher than the permitted overload.

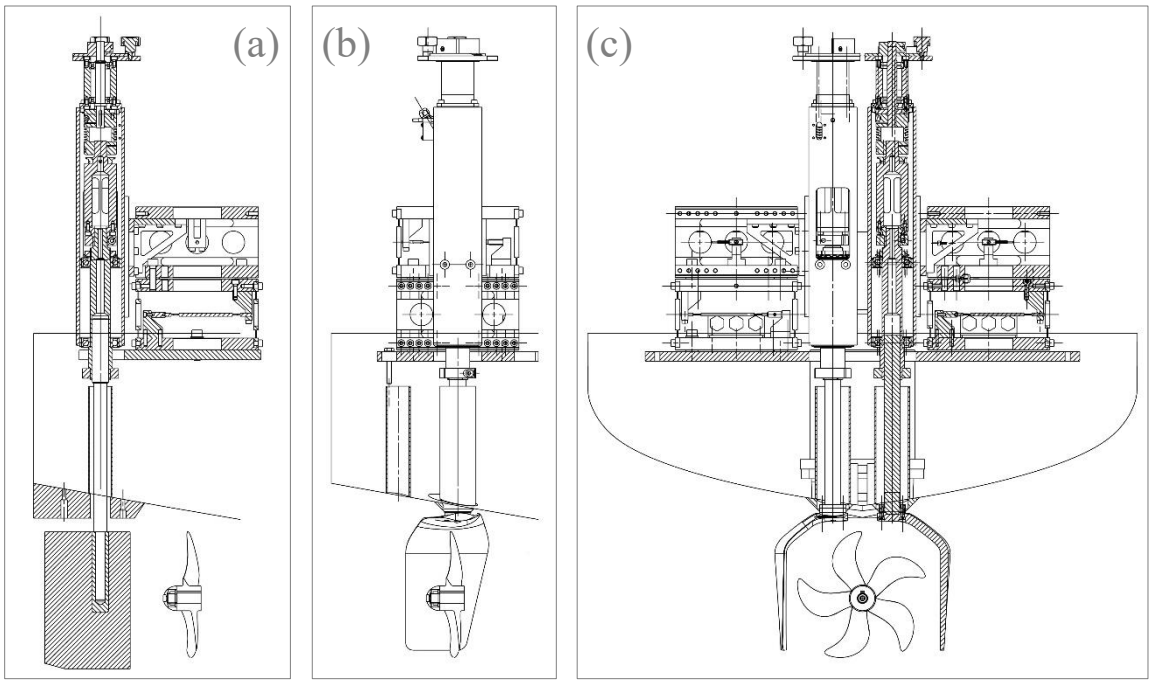

Fig. 3 Rudder force and moment measurement device setup in (a) the CRS, (b) and (c) the GRS configurations.

2.2 Model tests, numerical analyses and sea trials procedure

The calm water and oblique wave tests took place in the KHL towing tank. In the context of self-propulsion tests, it is necessary to consider an additional towing force to accurately determine the full-scale ship's propulsion characteristics. This external force, denoted as F_D, commonly referred to as the Skin Friction Correction (SFC), to compensate for variation in the Reynolds numbers (Re) between the model and the full-scale ship. The calculation of F_D is outlined in Eq. (1), following the guidelines given by ITTC (2017 b).

$$F_D = \frac{1}{2}\rho S V^2[(1+k)(C_{FS} - C_{FM}) - \Delta C_F] \quad (1)$$

The open-water tests were conducted in the towing tank of CTO S.A (CTO, 2022). at a Reynolds (Re) number to be greater than 2×10^5, at a constant propeller speed of 35 1/s under various flow speeds up to 5 m/s, to avoid the scale effect, according to the ITTC (2014). These tests, with the propeller (Fig. 4 a), were performed in open water conditions to determine the thrust (K_T) and torque (K_Q) coefficients as well as the efficiency of the propeller (η_0) and then with a dummy hub, without the propeller (Fig. 4 b), to be able to correct the propeller open water test results for the effects on thrust and torque of the hub, hub cap and aft fairing piece, thus yielding the open water characteristics of only the propeller blades.

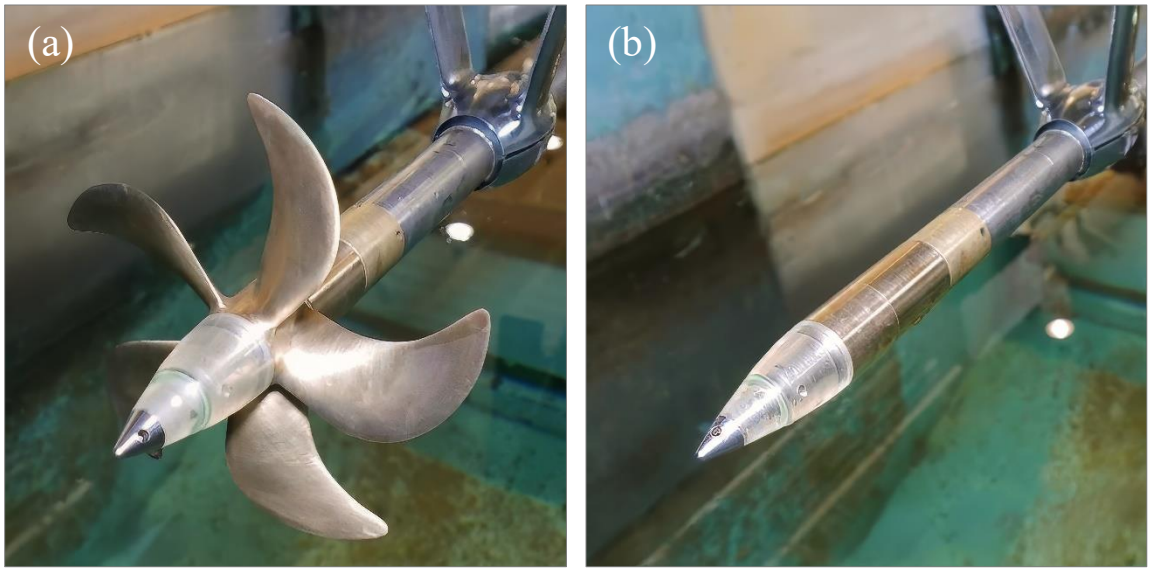

Fig. 4 Open water test setup with (a) propeller and (b) dummy hub.

The full-scale propeller performance characteristics were calculated using the model propeller data and geometric features, which were corrected for the scale effect according to the 1978 ITTC performance prediction procedure (ITTC, 2017 c).

The Reynolds-averaged Navier–Stokes (RANS) equations were utilised in the numerical analyses with the SST (Shear Stress Transport) k-ω turbulence model based on the Boussinesq hypothesis (Tennekes and Lumley, 1972). A segregated algorithm was used with the finite-volume method (Blazek, 2001) to solve the momentum and turbulent transport equations. The pressure-correction-based SIMPLE technique (Patankar and Spalding, 1972) was used to couple the pressure and velocity fields. The spatial discretisation of the convective terms of the Navier-Stokes and turbulent transport equations was acquired with a second-order-upwind scheme (Davidson, 2005), whilst a bounded central differencing scheme was used for the viscous terms.

The computational domain size ($5\times D_P$ to inlet, $10\times D_P$ to outlet, $5\times D_P$ to right and left sides, top and bottom) used in the simulations was determined following the ITTC (2014) procedure. In Fig. 5 (a), velocity inlet and pressure outlet conditions were defined for the boundaries' (+) x direction and (-) x direction, respectively. The symmetry condition was defined for the circular region between the velocity inlet and pressure outlet boundaries. The no-slip wall condition was specified for the propeller, shaft, hub and hub cap (yellow-coloured). The interface boundary condition was defined for the red-coloured rotating region in Fig. 5 (b) within the computational domain to transfer the information from one cell zone to another. In order to model the relative motion of the moving zone concerning adjacent zones (i.e., static region), the Multiple Reference Frame (MRF) model was adopted at first to accelerate the convergence of the solution; then, the propeller's rotation was simulated by switching the relative motion to the Sliding Mesh (SM) model. A trimmer-type mesh to generate an unstructured hexahedral-type grid structure, derived by the STAR-CCM+ meshing tool (Fig. 5, c), provides a robust and efficient approach to creating high-quality grids, addressing both straightforward and intricate mesh generation.

The height of the first cell along the prism layer was defined concerning the dimensionless wall distance, $y^+\sim50$, to model the boundary layer in full-scale analyses (Fig. 5, d). One might argue that using a low y^+ value could provide a more accurate representation of the flow field by resolving the boundary layer rather than modelling it. The decision to maintain a y^+ of around 50 was due to the simulations being conducted at full scale, where resolving the boundary layer would have required significantly more computational time, which was limited by capacity. A systematic series of grid densities refined by a constant ratio, $\sqrt[4]{2}$, was used to quantify the numerical uncertainty through validation and verification analyses in open-water conditions. In order to evaluate the grid-independency level, Richards Extrapolation-based Grid Convergence Index (GCI) as applied in CFD calculations (Song et al., 2021), relies on the principles of Richards Extrapolation, originally proposed by Richardson and Gant (1927), and Richardson et al. (1911). The GCI is computed following the methodology described by Celik et al. (2008). All validation and verification studies for the numerical analyses are given in GATERS Task 1.4 (2023).

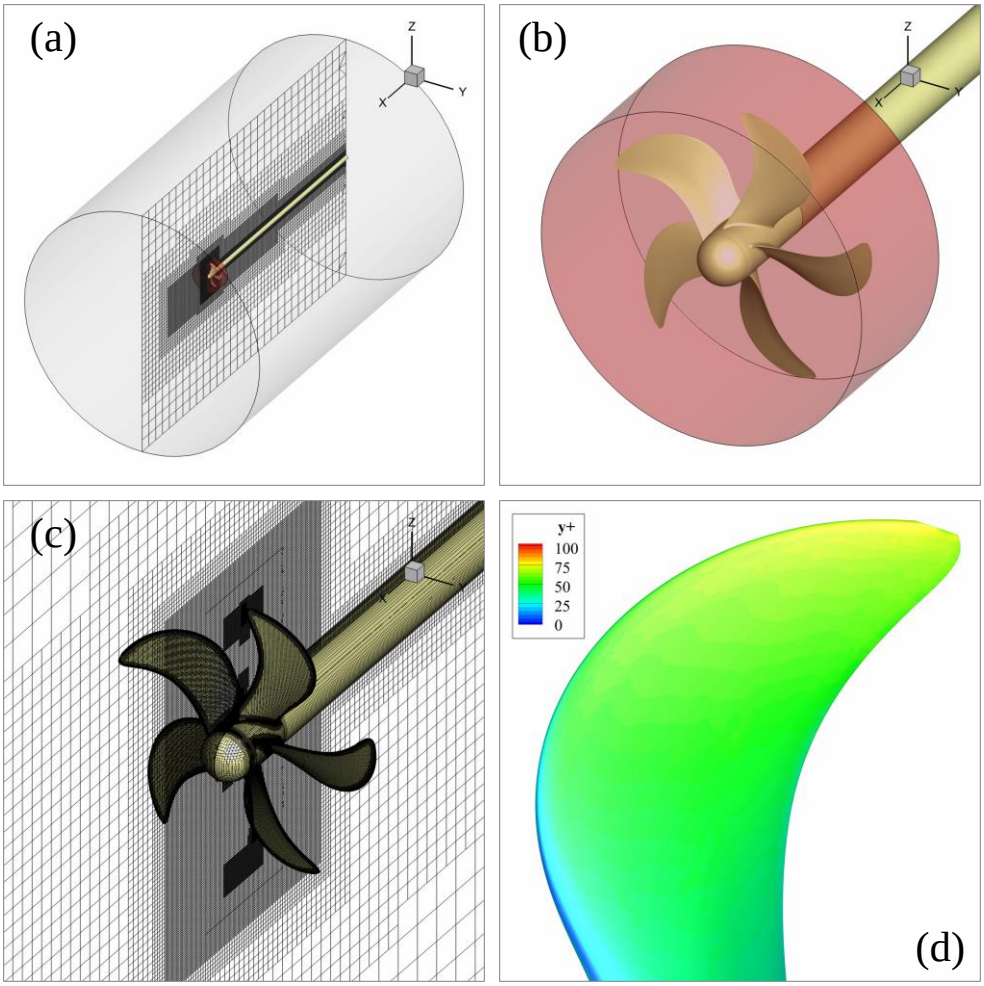

Fig. 5. (a) Computational domain size (5×D_P to inlet, 10×D_P to outlet, 5×D_P to right and left sides, top and bottom), (b) rotating domain, (c) representation of surface and volume mesh around the propeller, (d) y+ distribution along the propeller blade in full scale.

The load of the full-scale propeller is obtained from:

$$\frac{K_{TS}}{J_S^2} = \frac{1}{N_P}\frac{S_S}{2D_S^2}\frac{C_T}{(1-t)(1-w_{TS})^2} \tag{2}$$

with this, K_T/J^2 as the input value, the full-scale advance coefficient J_{TS} and torque coefficient K_{QTS} are read off from the full-scale propeller characteristics, and further performance data were calculated as follows.

Propeller rate of revolution (n_S) is

$$n_S = \frac{(1 - w_{TS})V_S}{J_{TS}D_S} \tag{3}$$

thrust of propeller (T_S) is

$$T_S = \frac{K_T}{J^2} J_{TS}^2 \rho_S {D_S}^4 {n_S}^2 \tag{4}$$

torque of propeller (Q_S) is

$$Q_S = \frac{K_{QTS}}{\eta_R} \rho_S {D_S}^5 {n_S}^2 \tag{5}$$

delivered power (P_D) is

$$P_D = 2\pi Q_S n_S \tag{6}$$

In the analysis of the ship with the CRS, the model wake fraction (w_{TM}) was converted to the full-scale wake fraction (w_{TS}) using the standard procedure (ITTC 2017 c).

$$w_{TS} = (t + w_R) + (w_{TM} - t - w_R)\frac{(1 + k)C_{FS} + \Delta C_F}{(1 + k)C_{FM}} \tag{7}$$

The effect of the rudders (w_R) on the wake fraction is taken as 0.04.

The leading computational and experimental investigations in the GATERS project (GATERS Task 2.1, 2024) and close collaborations with one of the GRS inventors, based on their experiences with limited full-scale sea trials in Japan implied the following pragmatic approximation, which is the model and full-scale wake flow are the same (Sasaki, 2022).

$$w_{TM} = w_{TS} \tag{8}$$

The calm water, resistance and self-propulsion, and oblique wave tests were conducted in the ballast load condition. The resistance tests were initially carried out with the bare hull configuration, without the propeller and rudder, and then repeated with the CRS and GRS configurations, without the propeller. The CRS and GRS were both considered an appendage, and the appendages resistance was extrapolated to the full scale using the beta factor (β), which is assumed to be 0.7 in line with the ITTC (2017 c). The form factor analysis was performed utilising

Prohaska's method for the ITTC 1978-based extrapolation procedure (ITTC, 2017 c). The air resistance was considered in the entire extrapolation analysis. The self-propulsion tests were conducted in calm water, free to trim and sink, while being constrained from surge, sway, and yaw. The GRS configuration involves the arrangement of individually controlled symmetrical twin rudders, like a controllable pitch propeller (CPP). According to Sasaki et al. (2015), the GRS' blades experience higher flow velocity on their inner surfaces facing the propeller than on their outer surfaces. This leads to a strong interaction between the GRS and the propeller, particularly as the angle of attack of the rudder increases with the rudder getting a higher toe-in angle (i.e., trailing edges of the rudders are getting far). The GRS was adopted to design angle, 0-degree, in the resistance and self-propulsion tests. Upon completion of the tests in the calm water, the ship model towing point attachment was modified to allow for the roll, in addition to the heave and pitch. Following the modification, a series of tests in the oblique waves were conducted in regular waves at the propeller shaft speeds, corresponding to the self-propulsion points of the CRS and GRS configurations. The oblique wave tests were conducted with the ship model oriented in the towing carriage at a mean yaw angle of 5 degrees oblique to the regular head waves for a range of different periods corresponding to Beaufort (BF) 4, as shown in Table 3, where H_S is the wave height, and T_S is the wave period both in full scale, ω_M is the wave (absolute) frequency in model scale, ω_e is encounter frequency and λ/L_{WL} is wavelength-to-ship length ratio. ω_e is greater than ω_M due to the tests being conducted at a yaw angle of the ship model in head waves.

Table 3. Test matrix in oblique waves.

V_S (knots)	H_S (meters)	T_S (s)	ω_M (Hz)	ω_e (Hz)	λ/L_{WL}
10	1.25	4.316	1.079	1.901	0.33 (BF 4)
10	1.25	5.273	0.883	1.433	0.50
10	1.25	6.458	0.721	1.088	0.75
10	1.25	7.457	0.625	0.900	1.00

M/V ERGE (Ex-JOERG N) is one of the eight sister multi-purpose dry-cargo ships initially commissioned and owned by a Germain Consortium. It was designed by a German design firm, ABH (ABH Ingenieur Technik GMBH) and was built by the Chinese shipyard Weihai Donghai. 7241 DWT multi-purpose dry-cargo, ship M/V ERGE, underwent a series of full-scale sea trials in 2010 before it was delivered. Following her build, the initial sea trials were carried out at the Yellow Sea of China in 2010. In 2023, another set of sea trials was conducted before replacing the CRS (Fig 6 a) with the GRS (Fig 6 b). Subsequently, the ship was docked to retrofit the GRS, and the hull was cleaned and painted. This was followed by further sea trials with the GRS retrofitted, which were conducted under the same loading conditions of the ship with the CRS. The sea trials of M/V ERGE with the CRS and GRS were performed on Marmara sea near Çınarcık in 2023. The dedicated onboard sea trials in the CRS and GRS configurations included speed-powering trials at varying engine loads as well as the circle manoeuvring and zig-zag tests. Ship's anemometer measured and recorded the relative wind directions and the wind speed, and a wave buoy was deployed in the sea trials area to obtain significant wave height and average wave period. Shaft speed (n) and torque (Q) measurements to obtain P_D, ship location through a GPS device, and fuel consumption through flowmeters were recorded and monitored in real-time during trials.

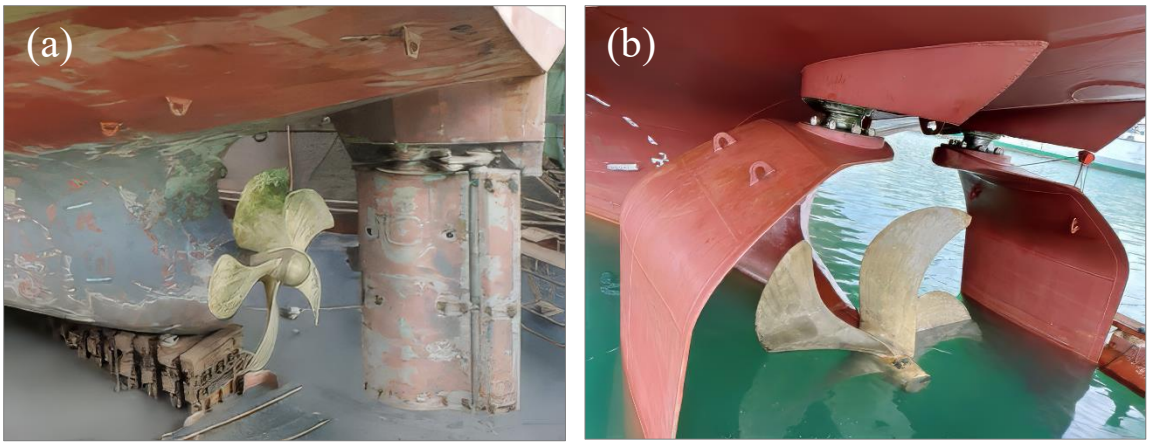

Fig. 6. M/V ERGE (a) before and (b) after the GRS retrofit.

The hull surface roughness measurements before and after the GRS retrofit in the dry dock in 2023, considering the ageing effect on the performance as the ship was not newly constructed. The roughness measurements conducted at the 120 positions using a hull roughness analyser (TQC) were thoroughly assessed to accurately report the hull roughness survey (Ravenna et al., 2023). One traverse of the head of the measurement device at any point on the hull collects information from 10 samples having a length of 50 mm (Eq. 9). For each 50 mm sample, the microprocessor assesses the mean gradient, known as $R_{t(50)}$, through the peaks and valleys to give the sample's highest peak to lowest valley measurements.

$$\mathrm{MHR} = \frac{1}{10}\sum_{i=1}^{10} R_{t(50)i}\,, \mathrm{AHR} = \frac{1}{120}\sum_{j=1}^{120} (\mathrm{MHR})_j \tag{9}$$

A method based on the ship length at the waterline (L_{WL}), surface roughness (k_s) and Reynolds number (Re) proposed by ITTC (2017 c) was utilised to consider the impact of the increase in the surface roughness of ships in a way, as shown in Eq. (10) below, where ΔC_F is the roughness allowance.

$$\Delta C_F = 0.044\left[\left(\frac{k_S}{L_{WL}}\right)^{\frac{1}{3}} - 10\mathrm{Re}^{-\frac{1}{3}}\right] + 0.000125 \tag{10}$$

The average hull roughness (AHR) of M/V ERGE was calculated as 300 μm using the mean hull roughness (MHR) measurements based on Eq. (9). In parallel with the measurements, the increase in hull surface roughness was assumed approximately 20 μm/year due to the ageing effect, and as a rule of thumb, every 20 μm of hull roughness adds 1% to the required propulsion power (Townsin, 1985). Therefore, the model test results in the GRS configuration were extrapolated to the full scale regarding the hull roughness measurements, k_S used as 300 μm, by Eq. (10) and Eq. (11), where k_S assumed to be 150 μm in the CRS configuration, newly constructed, following the ITTC (2017 c) procedure.

$$C_{TS} = (1 + k)C_{FS} + \Delta C_F + C_A + C_R + C_{AAS} \quad (11)$$

where C_{TS} is the total resistance coefficient of a ship without the bilge keel, k is the form factor determined from the resistance tests, C_{FS} is the frictional resistance coefficient of the ship, C_A is the correlation allowance, C_R is the residual resistance coefficient calculated from the total and frictional resistance coefficients of the model in the resistance tests and C_{AAS} is the air resistance coefficient in full scale.

3. Results and Discussions

The results for the propeller open water curves obtained by model tests (Fig. 7, a), model test results extrapolated to full scale according to the 1978 ITTC performance prediction procedure (ITTC, 2017 c), full scale numerical analyses and the design data used for the propeller retrofitted on the vessel, M/V ERGE (Fig. 7, b). The design data for the propeller was obtained using a method based on the Quasi-Continuous Vortex Lattice Method (QCM) (e.g., Streckwall, 1997), supplemented with empirical corrections.

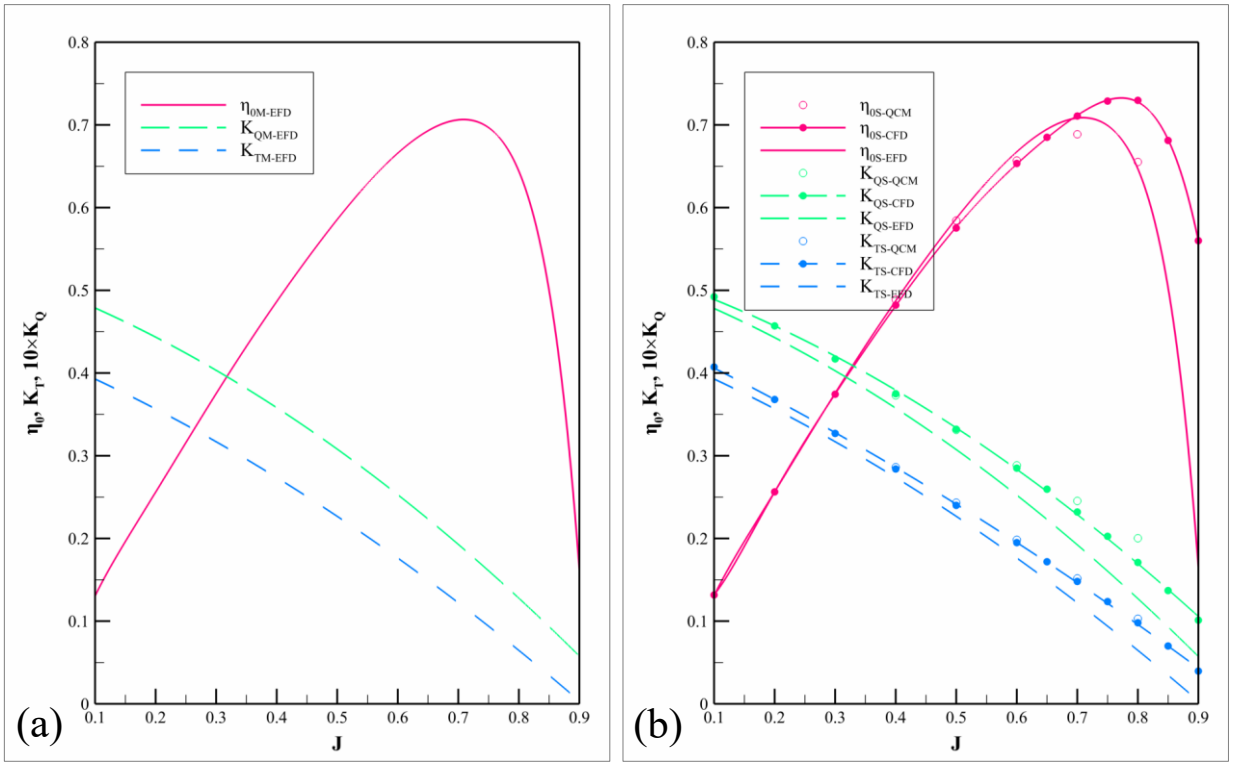

Fig. 7 Propeller open water curves, obtained by (a) model tests (EFD) and given in model scale (CTO, 2022), (b) extrapolating model test results to full scale using standard methods, numerical analyses in full scale (CFD) and the design data (QCM) used for the propeller.

Self-propulsion test results were extrapolated to ship scale based on full-scale numerical analysis of the propeller due to their compliance with the design data used for the propeller retrofitted on the vessel (Fig. 7, b). Additionally, there were concerns about the adequacy of standard methods given the unconventional geometrical features of the newly designed NPT (New Profile Technology) propeller (Carchen et al, 2015) of M/V ERGE (GATERS Task 2.1, 2024). The discrepancies in model and full-scale results obtained by experimental, computational, and empirical methods, as well as the influence of various numerical methods on the results, are not considered in this study. The primary objective is to evaluate the hull, propeller, and rudder interaction in calm water and waves, and addressing those discrepancies could form the basis of an entirely separate study.

Using the above-outlined procedure, in Section 2.2, the effective power (P_E) and delivered power (P_D) of M/V ERGE with the CRS and GRS configurations were extrapolated to full-scale from the model test results and plotted in Fig. 8 (a) and Fig. 8 (b), respectively. As shown in this figure, the GRS significantly reduced the power requirement of the ship at the same speed. There is a 5% effective power reduction at the service speed, 12 knots, for the hull with the GRS compared to the CRS. Therefore, the first initiative to refer to the superiority of the GRS and hull interaction might be to discuss the effective power comparison in both configurations. The self-propulsion test results obtained in the ballast load condition for the hull with the CRS (rudder amidship) and the GRS design angle at 0-degree configuration reveal that the GRS improves the energy efficiency for up to 12%, and the power saving (P_D) is almost 10% at the service speed, to the CRS (Table 4).

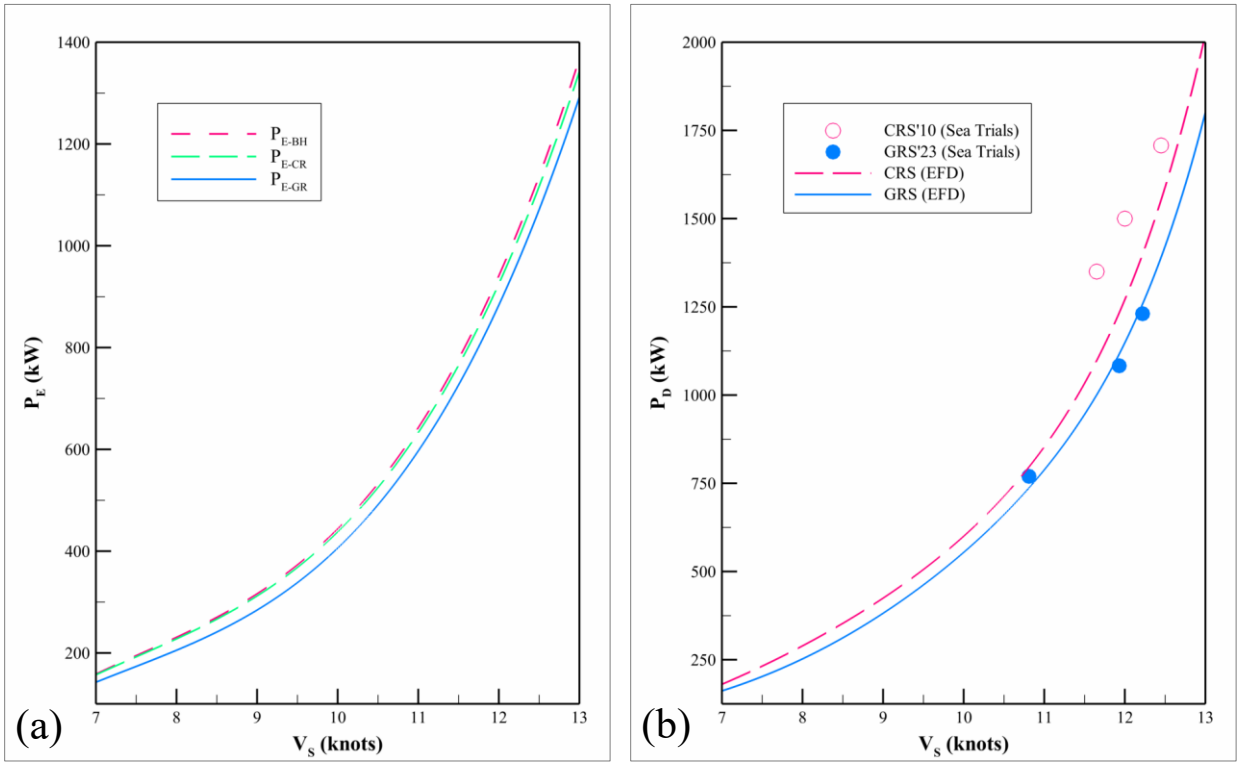

Fig. 8 (a) Effective and (b) delivered power predictions and their comparison with sea trials in both configurations.

Table 4. Self-propulsion characteristics of M/V ERGE at design speed, V_S=12 knots.

RS	P_E (kW)	w_{TS}	t	η_H	η_0	η_R	η_D	P_D (kW)
CRS	901.5	0.374	0.214	1.255	0.580	1.003	0.731	1234
GRS	856.6	0.226	0.134	1.119	0.655	1.044	0.765	1119

The relative rotative efficiency (η_R), as defined by Eq. (12), accounts for the differences in torque absorption characteristics of a propeller when operating in behind-ship and open-water conditions. In many cases, the value of η_R lies close to unity and is generally within the range of 0.95 and 1.05 (Carlton, 2007), as demonstrated by the findings of this study (Table 4). The procedure to calculate η_R is the same for both the CRS and GRS configurations, in accordance with the 1978 ITTC performance prediction method (ITTC, 2017 c), using thrust identity with propeller thrust coefficient at the model's self-propulsion point (K_{TM}) as input data, propeller advance coefficient achieved by thrust identity (J_{TM}) and torque coefficient achieved by thrust identity (K_{QTM}) are read off from the model propeller open water diagram. The GRS reduces the propeller load at the self-propulsion point and, consequently, K_{TM}, which leads to an increase in J_{TM} and a decrease in K_{QTM}, as achieved by thrust identity, compared to the CRS. The propeller torque coefficient at the model's self-propulsion point (K_{QM}) for the GRS is also lower than that for the CRS. However, the GRS' η_R is greater than the CRS' (Table 4) because the decrease in K_{QTM} is less than the decrease in K_{QM} for the GRS compared to the CRS. This suggests that the GRS reduces the propeller thrust more than the propeller torque at the self-propulsion point compared to the CRS.

$$\eta_R = \frac{K_{QTM}}{K_{QM}} \tag{12}$$

The thrust deduction factor (t), wake fraction (w_T), and the open water efficiency (η_0) have significant roles in defining the rest of the self-propulsion characteristics, such as η_H, η_R, η_D, P_D. The thrust deduction factor, as defined in Eq. (13), where T_M is propeller thrust, F_D is the skin friction correction force, and R_C is the resistance corrected for temperature differences between resistance and self-propulsion tests, is calculated the same way for both the CRS and GRS configurations. That being said, the authors are considering whether a revision to the standard full-scale extrapolation procedure of the thrust deduction factor obtained by model tests would improve accuracy, similar to the proposed modification on the extrapolation of the wake fraction. This will be explored in detail and summarised in due course as more data from model tests, sea trials, and voyage monitoring with the GRS are collected. The common argument is that the wake fraction is affected by waves compared to calm water conditions due to unsteady and periodically changing flow, wave-induced motion, flow separation, and vortex shedding, while it is assumed that the thrust deduction factor is only slightly affected by ship motions. In order to observe the variations in these characteristics, the results in the CRS and GRS configurations at the service speed are listed in Table 4. Here, the η_H calculated in the CRS exhibited a slight increase when compared to those determined in the GRS, which results in improved propulsive efficiencies (η_D) in general. However, the η_O of the GRS at the self-propulsion point is higher than the η_O of the propeller's open water data for the CRS. Therefore, the values of calculated η_D are higher for the GRS to the CRS, mainly due to the favourable propeller efficiency.

$$t = \frac{T_M - F_D - R_C}{T_M} \tag{13}$$

The corrected sea trial measurements analysed according to the ISO 15016 (ISO, 2015) procedure for the ship with the CRS in 2010 are depicted in Fig. 8 (b), along with the sea trial measurements in 2023 for the GRS. A detailed investigation of the measurements has yet to be reported, but real-time monitoring of the ship's performance during the sea trials revealed the GRS influence on fuel consumption at various rudder angles, as expected, leading to the decision to adopt an 8-degree toe-out angle (i.e., trailing edges of the rudders are getting closer) as a reference point for the GRS configuration. As shown in Fig. 8 (b), the speed range of the sea trials in 2010, which was conducted in the China Sea when the vessel was new, deviates from those conducted in 2023 mainly due to 13 years of ageing, both the hull and the engine. It can be observed that the ship retrofitted with the GRS displayed significantly reduced delivered power demand, up to 25%, as far as the lowest speed of the CRS in 2010 and the highest speed of the GRS in 2023 are concerned. However, it is evident that the model test results extrapolated to full scale for the CRS configuration moderately underestimated the 2010 sea trials, while the results for the GRS extrapolation slightly overestimated the 2023 sea trials. One reason to explain this discrepancy is that the same propeller was used in model tests for both the CRS and GRS configurations. In contrast, M/V ERGE was retrofitted with a newly built propeller in 2023 to accommodate the decreased propeller load due to the GRS's contribution to hull efficiency. Additionally, the GRS angle was set to 0 degrees during the model tests and 8 degrees during the sea trials, complicating direct side-by-side comparisons. Furthermore, there is still a gap to close for further accurate power predictions of ships with the GRS, as well as the need for more full-scale data for ships with the GRS. Consequently, the power savings of the GRS are almost half as much concerning the model test results compared to the sea trials. To investigate the hull, propeller, and rudder interaction in the self-propulsion tests, a tailor-made measurement device described in Section 2 was used for both the CRS and GRS configurations. The forces acting on the rudder blades (F_R) at the same model speed, various propeller speeds, and at the self-propulsion point of the ship model at different speeds are shown in Fig. 9 and Fig. 10 (a), respectively.

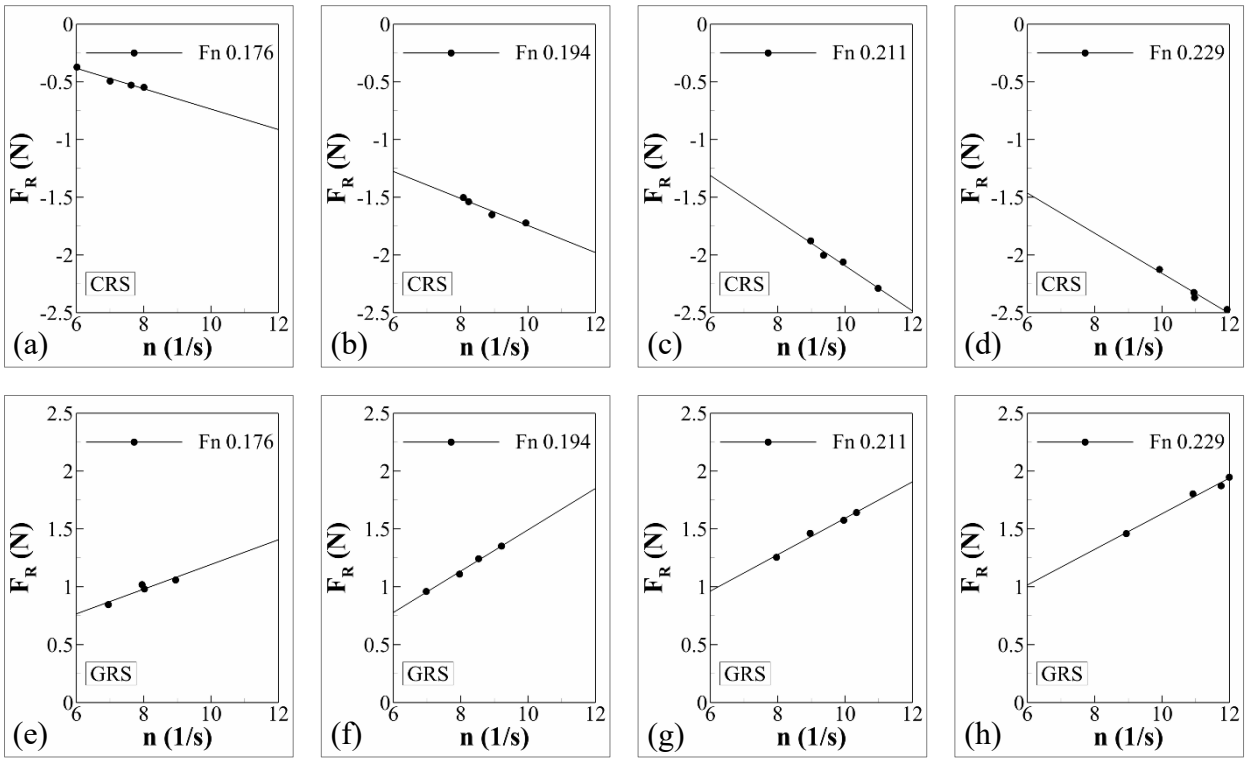

Fig. 9 The forces acting on the rudder blades at the same model speed in various propeller speeds, in (a), (b), (c) and (d) the CRS and (e), (f), (g) and (h) the GRS configurations.

As a result of the measurements, it was observed that when the ship speed is constant and the propeller speed increases, the rudder drag increases for the CRS, whereas the lift provided by the GRS increases (Fig. 9). Therefore, it is apparent that in a rough sea condition, a ship that increases its propeller speed to maintain ship speed or has to sail at a lower ship speed at the same propeller speed will cause an increment in the CRS' drag. In contrast, the GRS will enhance the ship's performance under the same conditions. Additionally, when examining the rudder forces at the self-propulsion point at different model speeds, it was determined that the GRS contributes more to the ship's performance as the ship speed increases. Again, the drag of the CRS increases, adversely affecting the ship's performance (Fig. 10, a). These results were obtained in calm water tests. Still, they may be treated as a reference for simulating either an increase in propeller speed to maintain ship speed in waves or maintaining propeller speed despite a decreased ship speed in waves. The strategy applied to engine control, whether increasing propeller speed or maintaining it in waves, is crucial for propeller performance and, consequently, the rudder and hull interaction. Therefore, the interaction of the engine control strategy with the hull, propeller, and rudder is a crucial parameter as far as the overall efficiency is concerned. Consequently, it can be concluded that, in terms of the interaction with the ship and propeller, GRS is superior to CRS based on the results of the calm water tests. In addition, the data provided in Fig. 9 and Fig. 10 (a) is supporting evidence of GRS' contribution to the performance in waves and, hence, to the engine control strategy, lowering the propeller load and improving the interaction of engine, hull, propeller and rudder.

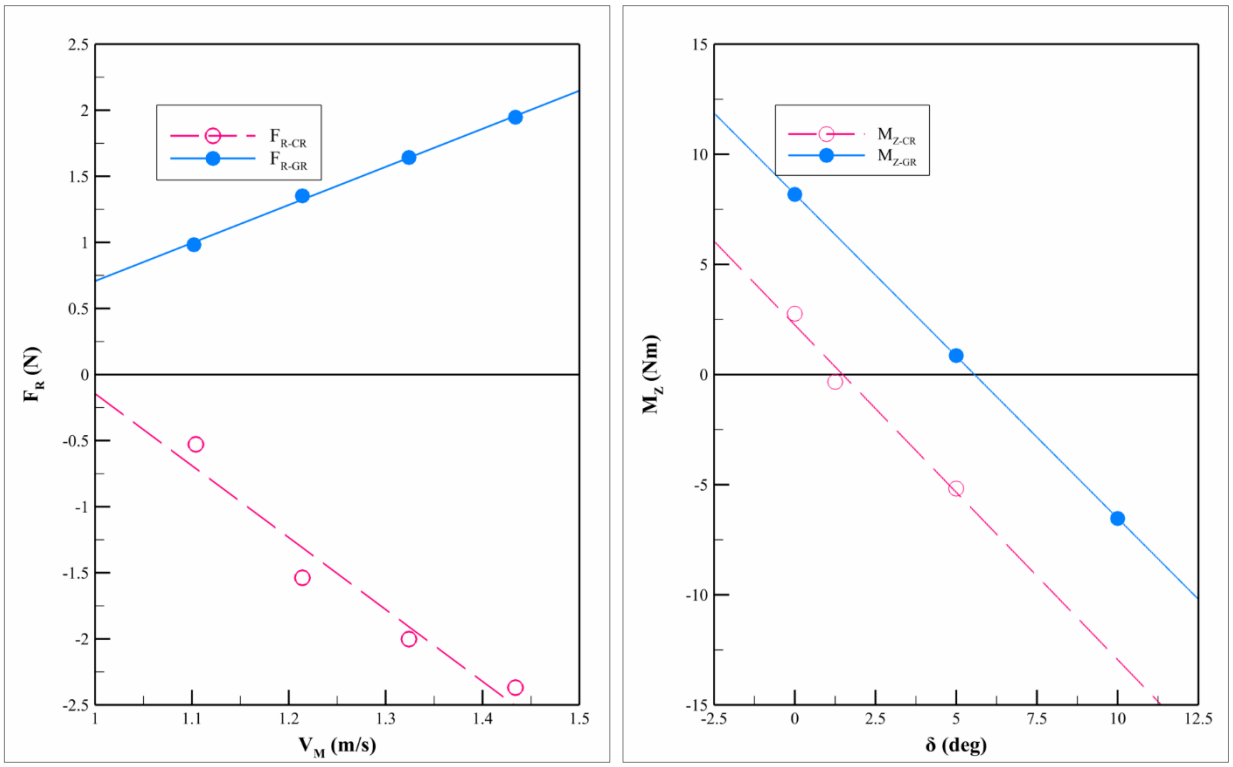

Fig. 10 (a) The forces acting on the rudder blades in various model speeds at their self-propulsion points. (b) Yaw moment of the ship model in different rudder angles in both configurations.

A series of model tests were conducted in various wave frequencies (ω_M), as given in Table 3, at a mean yaw angle of the ship model, 5 degrees, to investigate the hull, propeller, and rudder interaction in the oblique waves for both the CRS and GRS configurations. Yaw moments at the ship model's attachment point to the carriage were measured, and the CRS and GRS angles, δ, were varied to achieve a zero yaw moment in both configurations, hence the ship model maintaining an average yaw angle of 5 degrees, and to avoid excessive force and moment that could damage the load cell. Initially, the CRS and GRS angles were determined at a critical wavelength-to-ship length ratio (i.e., $\lambda/L_{WL}=1$, $\omega_e=0.9$ Hz) to achieve a zero yaw moment, and these rudder angles were kept the same for the rest of the tests in oblique waves. The tests in oblique waves were limited to $V_S=10$ knots because it was argued that the free surface elevation could exceed the freeboard, causing a large amount of water to flow into the ship model leading to failure. A steady yaw angle of 5 degrees of the ship model succeeded when the CRS rudder angle was 1.25 degrees, while the GRS rudder angles, both the port and starboard sides, were at 5 degrees as shown in Fig. 10 (b).

In the self-propulsion tests, the resultant force is a combination of the ship model resistance (R_T) due to normal and tangential shear forces on the hull, the propeller thrust (T), the drag or lift of appendages such as the CRS and GRS (F_R), and their interaction which will be referred to as F_i in this study (Fig. 11). The resultant force is also influenced by the added resistance (R_{AW}) in waves due to ship motion and the wave reflection.

The GRS is a novel energy-saving device recently introduced to the maritime industry. As with any emerging technology, comprehensive research is essential to understand its working principles, especially the extrapolation procedure for power predictions. Due to its unconventional configuration, conventional power prediction methods may not adequately capture the extrapolation characteristics for powering calculations. The treatment of the GRS as the appendage (Çelik, 2022), but not the propulsor unit, as well as the pragmatic wake assumption, $w_{TS}=w_{TM}$, were adopted in this study, acknowledging there is still some gap to close for further accurate power predictions of ships with the GRS, as well as more full-scale data. Therefore, both the drag and lift of the CRS and GRS (F_R) were assumed as part of R_T. The forces F_X, T, and only R_T (both for the CRS and GRS configurations, without the propeller), but not F_R, were considered in obtaining F_i (Eq. 14), similar to the numerator of the thrust deduction factor, where F_X is equal to F_D, commonly referred to as the Skin Friction Correction (SFC), in the self-propulsion tests.

$$F_i = T + F_X - R_T \tag{14}$$

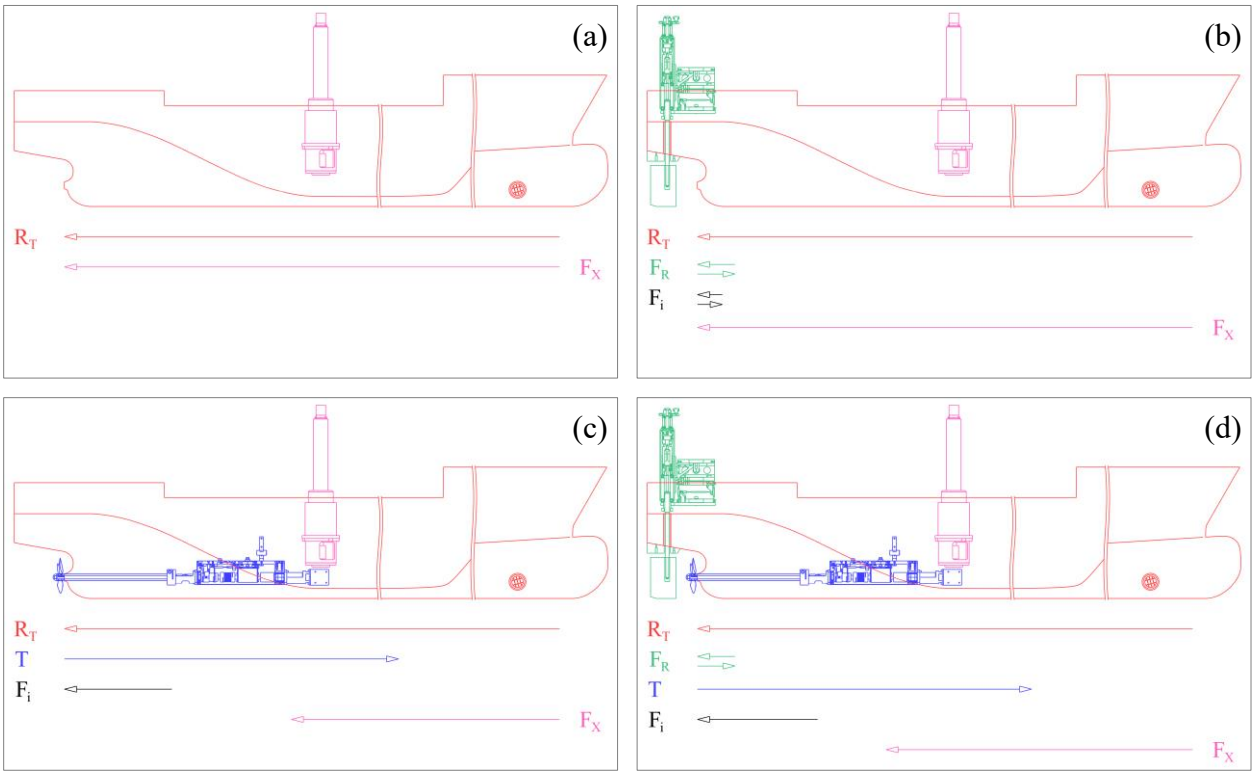

Fig. 11 Representation of (a) resistance tests, (b) hull and rudder interaction, (c) hull and propeller interaction and (d) hull, propeller and rudder interaction.

A comparison of the F_i values, using Eq. 14, in calm water and oblique waves for the CRS and GRS configurations is provided in Fig. 12 to assess the hull, propeller, and rudder interaction. It is evident that F_i in oblique waves is higher than in calm water due to the added wave resistance. In the comparison, the difference in F_i due to the added wave resistance is not accounted, as the ship motions in oblique waves were found to be similar for both CRS and GRS configurations in the model tests. However, Sasaki et al. (2021) demonstrated that the GRS reduced roll motion by up

to 2 degrees compared to the CRS, based on the joint sea trials of sister ships, SAKURA and SHIGENOBU, one with the CRS and the other with the GRS. Ship motion reduction in rough waves could not be measured in the model tests and this may be attributed to the scale effect. Having said that, no joint sea trials were conducted for M/V ERGE, highlighting more model scale and full-scale data is required to conclude the GRS's impact on the ship motions.

The GRS reduces the F_i by over 10% compared to the CRS, as shown in Fig. 12 (a) and Fig. 12 (c), indicating that the GRS's interaction with the hull and propeller is better than that of the CRS in calm water condition. This improvement is less pronounced in oblique waves, likely due to the influence of added wave resistance, but the GRS still reduces the F_i by 2.5% to 7.5% (Fig. 12 d). In oblique wave condition, the maximum interaction occurs at the highest wavelength-to-ship length ratio (i.e., λ/L_{WL}=1, ω_e=0.9 Hz) as seen in Fig. 12 (b). Consequently, it can be concluded that the thrust deduction factor will be reduced in oblique waves as well for the GRS configuration, considering its effect on the added resistance due to the hull, propeller and hull interaction, aligning with the self-propulsion test results.

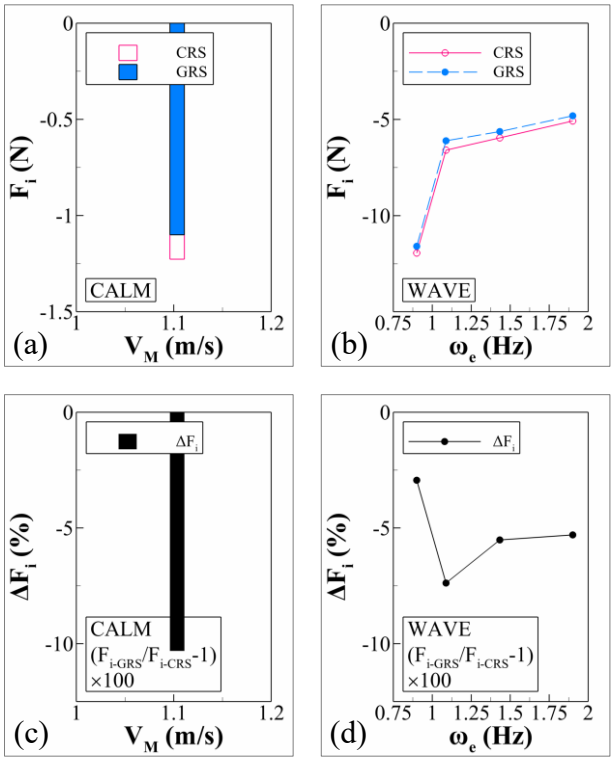

Fig. 12 Interaction in (a) and (c) calm water and (b) and (d) oblique waves for both configurations.

In addition to the investigation of F_i, the rudder force (F_R) measurements were also examined in calm water and oblique waves for the CRS and GRS configurations, as shown in Fig. 13 (d and h). Additionally, the forces on both GRS blades (Fig. 13 c and g), on the port (Fig. 13 a and e) and starboard (Fig. 13 b and f) sides, were given separately in Fig. 13 to assess the performance of each rudder blade at a yaw angle of the ship model in oblique waves. As explained in Section 2, the tests in oblique waves were conducted concerning the same propeller speed for each of the

CRS and GRS configuration self-propulsion points at V_S=10 knots. The most prominent finding of the comparison that is made between calm water and oblique waves is the dramatic increment of the CRS drag, over five times, in oblique waves compared to its drag in calm water (Fig. 13 i). However, the GRS is increasing its lift and improving the ship's performance even under oblique waves, as shown in Fig. 13 (j, k and l). It is also worth noting that both GRS blades increased their lift in oblique waves compared to calm water conditions, but the port side blade generates slightly more lift than the starboard side blade (Fig. 13 j and k), which may be related to the left-handed propeller rotation affecting the angle of attack on the rudder blades.

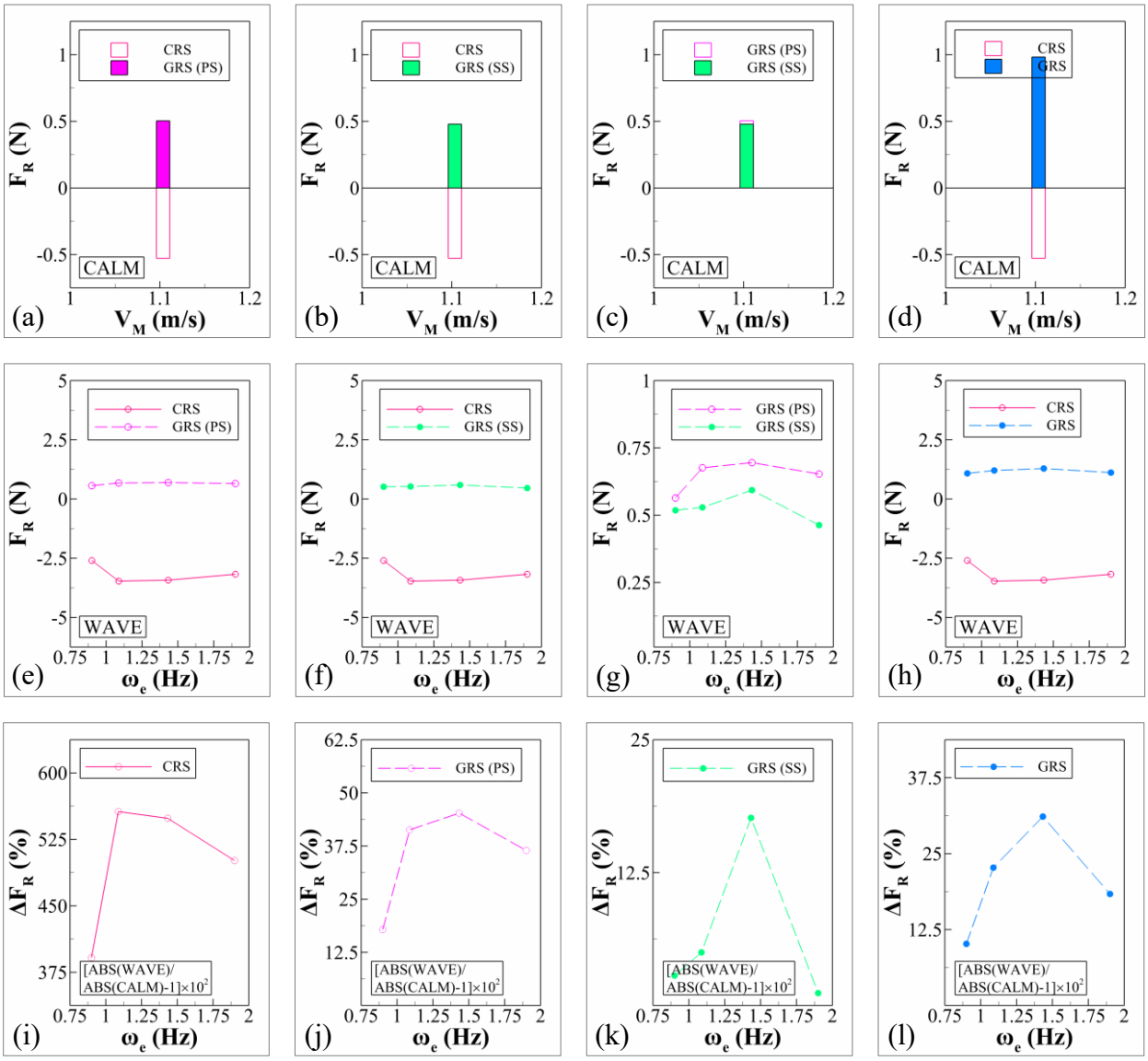

Fig. 13 Rudder force (F_R) in (a), (b), (c), (d) calm water condition and (e), (f), (g), (h) oblique waves, and (a), (b), (c), (d) their comparison for both the CRS and GRS configurations.

The comparison of propeller thrust (T) and propeller torque (Q) in calm water and oblique waves is presented in Fig. 14. Thrust and torque were in different trends in oblique waves for the CRS (Fig. 14 a and d) and GRS (Fig. 14 b and e) configurations. The propeller loading increased for the CRS but decreased for the GRS, indicating that the GRS increased propeller inflow speed in oblique waves compared to the calm water condition (Fig. 14 c and f). In contrast, propeller inflow speed decreased for the CRS configuration in oblique waves, leading to increased propeller loading. It is also worth mentioning that no correlation could be observed between the change in propeller loading and the encounter frequency in oblique waves.

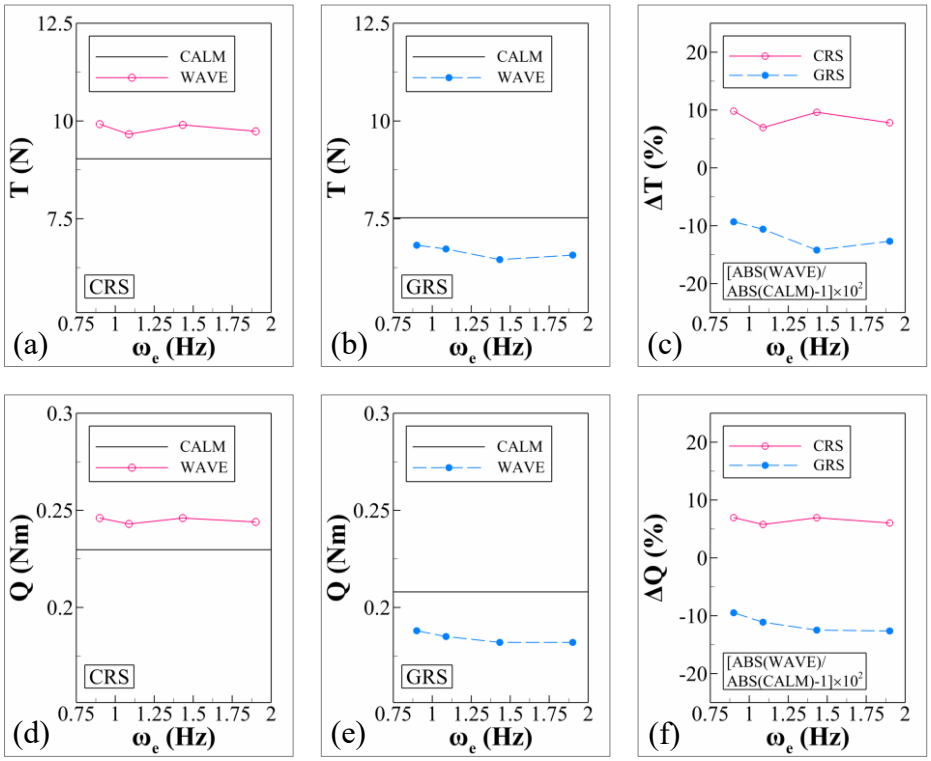

Fig. 14 Propeller thrust (T) and propeller torque in (a), (d) the CRS and (b), (e) GRS configurations, and (c), (f) their comparison.

4. Conclusions

The interaction of the hull, propeller, and both the CRS and GRS configurations in calm water and oblique waves (at a yaw angle of the ship model) was investigated experimentally to contribute to establishing the best procedure to estimate the performance of a ship, newly built or retrofitted with the GRS. The performance predictions based on the model tests were compared with sea trials in this respect. The rudder forces acting on both the CRS and GRS configurations were measured in calm water and oblique waves for the first time to assess the hull, propeller and rudder interaction. Tests in oblique waves were conducted at a single wave height, H_S=1.25 meters, for a range of wavelengths, λ=0.33, 0.50, 0.75 and 1, and at V_S=10 knots concerning the limits of the experimental setup, which were obtained based on the preliminary tests to avoid excessive forces and moments that could damage the load cell and to prevent the free surface elevation from exceeding the freeboard, which could cause a large amount of water to flow into the ship model

and lead to failure. In the oblique wave tests, the ship model was adjusted to a 5-degree yaw angle in both configurations, and no other configurations were analysed. This is also due to the nature of the experimental setup, which results in a yaw moment at the ship model's attachment to the carriage, and resolving this requires additional tests and a significant amount of time at the testing facility to determine and set the rudder angles needed to eliminate the yaw moment. Therefore, the overall energy that is to be recovered by the GRS, not only in oblique waves but also in calm water conditions, requires further model tests, sea trials and voyage monitoring data. Based on the investigation presented in the paper, the following conclusions can be drawn.

- The interaction of the GRS with the hull and propeller was found to be superior in both calm water and oblique waves, corresponding to moderate breeze, Beaufort 4, wave height of 1.25 meters in full scale, compared to the CRS. In the CRS configuration, the rudder drag increased dramatically by a factor of 5. In contrast, the GRS improved the ship's performance, decreasing the propeller load and increasing the rudder lift at a 5-degree yaw angle of the ship model. These results complement the findings presented by Sasaki et al. (2021), which indicated that the GRS significantly improved ship performance in rough seas, based on joint sea trials of a container ship with the CRS and her sister ship with the GRS. Additionally, improving the performance in rough seas aligns with the voyage monitoring data of M/V ERGE following her retrofit with the GRS.
- Model tests in calm water demonstrated that the GRS reduced ship resistance by 5% and power consumption by over 10% compared to the CRS. Additionally, in oblique waves at a 5-degree yaw angle of the ship model, the GRS decreased propeller loading by increasing the propeller inflow speed compared to the CRS. Consequently, propeller designs for ships with the GRS will require further attention and more data regarding this aspect in comparison to the design of the CRS propellers.
- Sea trials and model test results demonstrated that the GRS significantly reduced power consumption by 25% and over 10%, respectively, compared to the CRS. These analyses indicate that the GRS is a major contender for the most effective energy-saving device for ships, applicable not only to new builds but also to existing ships as a retrofit. However, there is still some gap to close for further accurate power predictions of ships with the GRS, as well as more full-scale data.
- Further steps to investigate the hull, propeller, and the GRS interaction, include, but are not limited to, extrapolating the model test results in waves to full scale, running numerical analyses at full scale, and ideally, installing sensors on the rudder blades. These sensors would be used to correlate power consumption, ship and propeller speed, and forces and moments acting on the rudder blades during various voyage conditions. Additionally, to enhance the model test results and comparison with sea trials, a further study is planned to conduct model tests using the actual propeller geometry in sea trials for the CRS and with an 8-degree rudder angle for the GRS case.
- As the pilot investigation regarding the effect of the oblique waves on the GRS performance, the current propulsion tests were conducted in a conventional towing tank, and the model was set at a small oblique heading angle to simulate the required wave condition. Ideally, these tests should be conducted in a large ocean basin with a free-running model tested at varying ranges of wave conditions. However, these pioneering tests were the first step toward this ultimate experimental work to be conducted in the future.

Acknowledgements

This paper is based on the activities conducted in the collaborative European project GATERS, which was an Innovation Action Project funded by the EC H2020 Programme (ID: 860337) with independent aims and objectives. The project had an official sub-license agreement with Wartsila Netherlands BV to utilise the Gate Rudder Patent (EP 3103715) at specific retrofit projects of vessel sizes below 15000 DWT.

References

Blazek, J. Computational Fluid Dynamics: Principles and Applications, third ed., Elsevier, Oxford, 2001, doi: 10.1016/C2013-0-19038-1.

Bulten, N., 2024. Upgraded MMG-Methodology to Capture Gate-Rudder Performance Aspects. Eighth International Symposium on Marine Propulsors, smp'24, Berlin, Germany. https://10.15480/882.9324.

Carchen, A., Sasaki, N., Aktas, B., Turkmen, S., Atlar, M., 2015. Design and Review of the New NPT Propeller for the Princess Royal. In 7th International Conference on Advanced Model Measurement Technology for the Maritime Industry. Istanbul, Türkiye.

Carchen, A., Turkmen, S., Piaggio, B., Shi, W., Sasaki, N., & Atlar, M., 2021. Investigation of the manoeuvrability characteristics of a Gate Rudder system using numerical, experimental, and full-scale techniques. Applied Ocean Research, 106, 102419. https://doi.org/10.1016/j.apor.2020.102419.

Carlton, J.S. Marine Propellers and Propulsion. part 2: Ship resistance and propulsion. Second Edition (2007), 286–318. https://doi.org/10.1016/B978-075068150-6/50014-0.

Çelik, C., Özsayan, S., Köksal, Ç.S., Danışman, D.B., Korkut, E., Gören, Ö., Atlar, M., 2023. On the Evaluation of the Model Test Extrapolation by Sea Trial Measurements. In 7th International Conference on Advanced Model Measurement Technology for the Maritime Industry. Istanbul, Türkiye.

Çelik, C., Özsayan, S., Köksal, Ç.S., Danışman, D.B., Korkut, E., Gören, Ö., 2022. On the Full-Scale Powering Extrapolation of Ships with Gate Rudder System (GRS). In A. Yücel Odabaşı Colloquium Series 4th International Meeting-Ship Design & Optimization and Energy Efficient Devices for Fuel Economy. Istanbul, Türkiye.

Celik, I. B., Ghia, U., Roache, P. J., Freitas, C. J., Colmena, H., & Raad, P. E. (2008). Procedure for estimation and reporting of uncertainty due to discretisation in CFD applications. Journal of Fluids Engineering-Transactions of the ASME 0078001-078001-4, 130(7).

CTO, Centrum Techniki Okrętowej S.A. Results of Hydrodynamic Characteristics Measurements of the Open Water Propeller Model, RH-2022/B-22145, 2022.

Davidson, L. Numerical Methods for Turbulent Flow, MTF071 Lecture Notes, Chalmers University of Technology, Goteborg, Sweden: Department of Thermo and Fluid Dynamics, 2005.

Fukazawa, M., Turkmen, S., Marino, A., Sasaki, N., November, 2018. Full-scale gate rudder performance obtained from voyage data. In Proceedings of the A. Yücel Odabaşı Colloquium Series: 3rd International Meeting-Progress in Propeller Cavitation and Its Consequences: Experimental and Computational Methods for Predictions, Istanbul, Turkey (pp. 15-16).

Gate Rudder System as a Retrofit for the Next Generation Propulsion and Steering of Ships, 2021. The EC - H2020 Project GATERS (Project ID: 860337). https://10.3030/860337.

Gate Rudder System as a Retrofit for the Next Generation Propulsion and Steering of Ships, 2024. Full-Scale Trials and Voyage Monitoring of the Target Ship in Task 2.1. The EC - H2020 Project GATERS (Project ID: 860337, 2021). Work Package 2.

Gate Rudder System as a Retrofit for the Next Generation Propulsion and Steering of Ships, 2023. CFD Based Performance Simulations Conducted in Task 1.4. The EC - H2020 Project GATERS (Project ID: 860337, 2021). Work Package 1.

Gate Rudder System as a Retrofit for the Next Generation Propulsion and Steering of Ships, 2022. Maximum Loading Conditions and Structural Assessment of Gate Rudder System for MV ERGE, TR1.1 05. The EC - H2020 Project GATERS (Project ID: 860337, 2021).

Guiard, T., Leonard, S., Mewis, F., May, 2013. The Becker Mewis Duct® - Challenges in Full-Scale Design and new Developments for Fast Ships. In 3rd International Symposium on Marine Propulsors, smp 2013, Tasmania, Australia.

Gürkan, A.Y., Köksal, Ç.S., Aktas, B., Ünal, U.O., Atlar, M., & Sasaki, N., 2023 (c). Computational Investigation of The Impact of a Gate Rudder System on A High Block Coefficient Coastal Vessel as A Retrofit. In 7th International Conference on Advanced Model Measurement Technology for the Maritime Industry. Istanbul, Türkiye.

Gürkan, A.Y., Turkmen, S., Sasaki, N., Aktas, B., Köksal, Ç.S., Atlar, M., 2023 (d). Manoeuvrability Improvement Investigation of a Coastal Vessel Retrofitted with A Gate Rudder System Using Computational and Experimental Methods. In 7th International Conference on Advanced Model Measurement Technology for the Maritime Industry. Istanbul, Türkiye.

Gürkan, A.Y., Ünal, U.O., Aktas, B., Atlar, M., 2023 (a). An investigation into the gate rudder system design for propulsive performance using design of experiment method. Ship Technology Research, 71(2), 199-212. https://doi.org/10.1080/09377255.2023.2248721.

Gürkan, A.Y., Ünal, U.O., Aktas, B., Köksal, Ç.S., Atlar, M., 2023 (b). Comprehensive Investigation of the Form Design of The Gate Rudder for Propulsive Performance Using Design of Experiment Method. 25th Numerical Towing Tank Symposium (NuTTS), Ericeira, Portugal.

H. Tennekes, J.L. Lumley, A First Course in Turbulence, MIT, Cambridge, 1972, doi: 10.7551/mitpress/3014.001.0001.

ISO 15016, 2015. Ships and Marine Technology d Guidelines for the Assessment of Speed and Power Performance by Analysis of Speed Trial Data.

ITTC, ITTC propulsion committee, in: Proceedings of the 28th International Towing Tank Conference, Recommended Procedures and Guidelines, Propulsion/Bollard Pull Test, 2017 (b), 7.5-02-03-01.1.

ITTC, ITTC propulsion committee, in: Proceedings of the 28th International Towing Tank Conference, Recommended Procedures and Guidelines, 1978 ITTC Performance Prediction Method, 2017 (c), 7.5-02-03-01.4.

ITTC, ITTC quality systems group, in: Proceedings of the 28th International Towing Tank Conference, Recommended Procedures and Guidelines, Open Water Test, 2014, 7.5-02-03-02.1.

ITTC, ITTC resistance committee, in: Proceedings of the 28th International Towing Tank Conference, Recommended Procedures and Guidelines, Ship Models, 2017 (a), 7.5-01-01-01.

ITTC. ITTC Specialist Committee on CFD in Marine Hydrodynamics. 27th International Towing Tank Conference, Recommended Procedures and Guidelines, Practical Guidelines for Ship Self-Propulsion CFD, 7.5-03-03-01, 2014.

Kitazawa, T., Hikino, M., Fujimoto, T., Ueda, K. (1982).Increase in the propulsive efficiency of a ship by anozzle installed just in front of a propeller. Journal of the Kansai Society of Naval Architects, 184, 73-7.

Köksal, Ç.S., Aktas, B., Gürkan, A.Y., Korkut, E., Sasaki, N., Atlar, M., 2022. Experimental Powering Performance Analysis of M/V ERGE in Calm Water and Waves. In A. Yücel Odabaşı Colloquium Series 4th International Meeting-Ship Design & Optimization and Energy Efficient Devices for Fuel Economy. Istanbul, Türkiye.

Köksal, Ç.S., Gürkan, A. Y., Aktas, B., Ünal, U.O., Fitzsimmons, P., Sasaki, N., Atlar, M., 2023 (a). Cavitation Observation of M/V ERGE During the Sea Trials: A Comparison of Gate Rudder and Conventional Rudder Configurations. In 7th International Conference on Advanced Model Measurement Technology for the Maritime Industry. Istanbul, Türkiye.

Köksal, Ç.S., Gürkan, A.Y., Aktas, B., Sasaki, N., Atlar, M., 2023 (c). Influence of Gate Rudder System (GRS) Rudder Angle(s) on the Propulsive Efficiency. 25th Numerical Towing Tank Symposium (NuTTS), Ericeira, Portugal.

Köksal, Ç.S., Gürkan, A.Y., Aktas, B., Turkmen, S., Zoet, P., Sasaki, N., Atlar, M., 2023 (b). Underwater Radiated Noise Measurements of Pre-and Post-Retrofit of Gate Rudder System During the Sea Trials. In 7th International Conference on Advanced Model Measurement Technology for the Maritime Industry. Istanbul, Türkiye.

Köksal, Ç.S., Gürkan, A.Y., Aktas, B., Ünal, U.O., Fitzimmons, P., Sasaki, N., Atlar, M., April, 2024. Quantifying the influence of Gate Rudder System (GRS) rudder angle (s) on propeller cavitation. In 8th International Symposium on Marine Propulsors, smp 2024, Berlin, Germany. https://10.15480/882.9364.

Mewis, F., Guiard, T., June, 2011. Mewis Duct® – New Developments, Solutions and Conclusions. In 2nd International Symposium on Marine Propulsors, smp 2011, Hamburg, Germany.

Mewis, F., June, 2009. A Novel Power-Saving Device for Full-Form Vessels. In 1st International Symposium on Marine Propulsors, smp 2009, Trondheim, Norway.

Mizzi, K., Zammit Munro, M., Gürkan, A.Y., Aktas, B., Atlar, M., Sasaki, N., 2022. The Performance Prediction and Energy Saving Evaluation for the Retrofit of a Gate Rudder System on a General Cargo Vessel using CFD Procedures. In A. Yücel Odabaşı Colloquium Series 4th International Meeting-Ship Design & Optimization and Energy Efficient Devices for Fuel Economy, Istanbul, Turkey.

Özsayan, S., Aydin, Ç., Koksal, Ç.S., Ünal, U.O., Korkut, E., 2023. Effects of the Gate Rudder System (GRS) on the Experimental Cavitation Observations and Noise Measurements. In 7th International Conference on Advanced Model Measurement Technology for the Maritime Industry. Istanbul, Türkiye.

Patankar, S.V. and Spalding, D.B. A Calculation Procedure for Heat, Mass and Momentum Transfer in Three-Dimensional Parabolic Flows. International Journal of Heat and Mass Transfer. 15, 1787-1806, 1972.

Propulsive Performance Using Design of Experiment Method. 25th Numerical Towing Tank Symposium (NuTTS), Ericeira, Portugal.

Ravenna, R., Özsayan, S., Köksal, Ç.S. and Atlar, M., 2023. M/V ERGE's Hull Fouling and Roughness Survey Report. The EC - H2020 Project GATERS (Project ID: 860337, 2021).

Richardson, L. F. (1911). The approximate arithmetical solution by finite differences of physical problems involving differential equations, with an application to the stresses in a masonry dam. Transactions of the Royal Society of London, 210(459-490).

Richardson, L. F., & Gant, J. A. (1927). The deferred approach to the limit. Transactions of the Royal Society of London, 226(636-646).

Santic, I., Mauro, S., Micci, G., Felli, M., 2023. Systematic Experimental Survey of Propulsive and Acoustic Performances of a Gate Rudder System in Relation to a Conventional Rudder. In 7th International Conference on Advanced Model Measurement Technology for the Maritime Industry. Istanbul, Türkiye.

Sasaki, N., & Atlar, M., 2024. Gate Rudder System and Ship Design. Eighth International Symposium on Marine Propulsors, smp'24, Berlin, Germany. https://10.15480/882.9301.

Sasaki, N., 2022. Private Communications on Powering Aspects of Ships With GRS.

Sasaki, N., Atlar, M., Kuribayashi, S., 2016. Advantages of twin rudder system with asymmetric wing section aside a propeller: the new hull form with twin rudders utilising duct effects. J. Mar. Sci. Technol. 21, 297–308.https://doi.org/10.1007/ s00773-015-0352-z.

Sasaki, N., Kuribayashi, S., Asaumi, N., Fukazawa, M., Nonaka, T., Turkmen, S., Atlar, M., October, 2017. Measurement and calculation of gate rudder performance. In The 5th International Conference on Advanced Model Measurement Technology for the Maritime Industry.

Sasaki, N., Kuribayashi, S., Bulten, N., Yazawa, M. 2021. Joint sea trial of ships with gate rudder and conventinal rudder. Royal Institution of Naval Architects (RINA)- Full Scale Ship Performance Conference. London, UK.

Sasaki, N., Kuribayashi, S., Fukazawa, M., Atlar, M., 2020. Towards a realistic estimation of the powering performance of a ship with a gate rudder system. Journal of Marine Science and Engineering, 8(1), 43. https://doi.org/10.3390/jmse8010043

Sasaki, N., Kuribayashi, S., Miles, A., 2019. Full scale performance of gate rudder. Royal Institution of Naval Architects (RINA)-Propellers and Impellers: Research, Design, Construction and Application. London, UK. https://doi.org/10.3940/rina.pro.2019.10.

Schneekluth, H. (1989). The wake equalising duct. International Maritime and Shipping Conference, 103, 147-150.

Simonsen, C., Nielsen, C., Klimt-Mollenbach, C., Holm, C. and Minchev, A. CFD based investigation of potential power saving for different rudder types, positions and pre-swirl fins, FORCE Technology, 2012.

Song, K., Guo, C., Sun, C., Wang, C., Gong, J., Li, P., & Wang, L. (2021). Simulation strategy of the full-scale ship resistance and propulsion performance. Engineering Applications of Computational Fluid Mechanics, 15(1).

Streckwall, H., "Description of a Vortex Lattice Method for Propellers in Steady and Non Steady Flow". (1997), Hamburgische Schiffbau-Versuchsanstalt GmbH: Hamburg.

Tacar, Z., Sasaki, N., Atlar, M., Korkut, E., 2020. An investigation into effects of Gate Rudder® system on ship performance as a novel energy-saving and manoeuvring device. Ocean Engineering, 218, 108250. https://doi.org/10.1016/j.oceaneng.2020.108250.

Tennekes, H. and Lumley, J.L. A First Course in Turbulence, MIT, Cambridge, 1972, doi: 10.7551/mitpress/3014.001.0001.

Townsin, R.L., 1985. The ITTC Line-Its Genesis and Correlation Allowance. The Naval Architect, London, UK.

Turkmen, S., Carchen, A., Sasaki, N., Atlar, M., November, 2015. A new energy saving twin rudder system-gate rudder. In SCC 2015 International Conference on Shipping in Changing Climates: Technologies, Operations, Logistics and Policies Towards Meeting 2050 Emission Targets.

Turkmen, S., Fukazawa, M., Sasaki, N., Atlar, M., 2018. Cavitation tunnel tests and full-scale review of the first gate rudder system installed on the 400TEU container ship. In A. Yücel Odabaşı Colloquium Series 3rd International Meeting on Progress in Propeller Cavitation and its Consequences: Experimental and Computational Methods for Predictions (pp. 29-39). Istanbul Turkey.